Available online at www.sciencedirect.com

Food and Bioproducts Processing

journal homepage: www.elsevier.com/locate/fbp

Jet cutter technique as a tool to achieve high lipase hydrolytic activity

Francisco Lucas Chaves Almeida[a,b,c,1], *Mariana Pereira Silveira*[c,2], *Izabela Dutra Alvim*[d,3], *Talles Barcelos da Costa*[e,4], *Thiago Lopes da Silva*[e,5], *Melissa Gurgel Adeodato Vieira*[e,6], *Ana Silvia Prata*[b,7], *Marcus Bruno Soares Forte*[a,b,*,8]

[a] *Interinstitutional Graduate Program in Bioenergy (USP/UNICAMP/UNESP), Rua Cora Coralina, 330, Cidade Universitária, Campinas, São Paulo, Brazil*

[b] *Metabolic and Bioprocess Engineering Laboratory, Department of Food Engineering and Technology, School of Food Engineering, University of Campinas, São Paulo, Brazil*

[c] *Laboratory of Food Innovation, Department of Food Engineering and Technology, Faculty of Food Engineering, University of Campinas, São Paulo, Brazil*

[d] *Cereal and Chocolate Technology Center, Cereal Chocotec, Institute of Food Technology, Ital, Campinas, São Paulo, Brazil*

[e] *Laboratory of Engineering and Environmental Processes, Department of Process and Product Design, School of Chemical Engineering, University of Campinas, São Paulo, Brazil*

ARTICLE INFO

Article history:
Received 9 June 2022
Received in revised form
15 November 2022
Accepted 2 December 2022
Available online 6 December 2022

Keywords:
Eversa
Transform 2.0
Entrapment
Enzyme immobilization

ABSTRACT

Lipase immobilization has been widely studied because it allows for enzyme reuse and provides more assertive control over the catalytic process. This study aimed to evaluate the effect of bead size on the performance of entrapped lipase. Eversa® Transform 2.0 was immobilized on calcium alginate beads by jet cutting and dripping. Beads produced by jet cutting were small ($D_{[3,4]}$ = 803.36 ± 16.9 μm) and had a relatively narrow size distribution (span of 0.79). Beads obtained by extrusion dripping measured 2459.98 ± 15.6 μm and had a span of 0.45. Infrared spectroscopy and microscopic analysis confirmed the presence of lipase in both types of beads. Lipase showed high hydrolytic activity in its free form (15,000 U g^{-1}). Immobilization in calcium alginate was effective but decreased recovered enzyme activity. The porosity of loaded beads varied with size. The high surface area (5.46 vs 3.13 m^2 g^{-1}) and porosity (76.33% vs 21.65%) of beads produced by jet cutting, as compared with those produced by dripping, favored enzyme activity (3000 vs 1500 U g^{-1} protein). The results indicate that facilitated mass transfer is an important factor in the development of immobilized enzymes.

* Corresponding author at: Interinstitutional Graduate Program in Bioenergy (USP/UNICAMP/UNESP), Rua Cora Coralina, 330, Cidade Universitária, Campinas, São Paulo, Brazil.
E-mail address: forte@unicamp.br (M.B.S. Forte).
[1] ORCID: 0000-0001-5349-7645
[2] ORCID: 0000-0002-0618-1872
[3] ORCID: 0000-0002-7882-5147
[4] ORCID: 0000-0002-4537-9750
[5] ORCID: 0000-0003-1880-7673
[6] ORCID: 0000-0002-3487-799X
[7] ORCID: 0000-0002-8421-0712
[8] ORCID: 0000-0002-2263-4392

https://doi.org/10.1016/j.fbp.2022.12.001
0960-3085/

1. Introduction

Lipases (triacylglycerol acyl hydrolases, EC 3.1.1.3) are a group of enzymes possessing a catalytic triad composed of a serine, a histidine, and an aspartate or glutamic acid residue (Fojan, 2000; Neves Petersen et al., 2001). These enzymes are extensively used in dairy, oil and fat, food, nanotechnology, and biofuel industries (Almeida et al., 2021a; Facin et al., 2019). However, in their free form, lipases have important disadvantages, such as high cost, high solubility, difficult reuse, and very low stability under extreme pH and temperature conditions (Badoei-dalfard et al., 2022; Guisan et al., 2022). Enzyme immobilization has emerged as a tool to solve these problems (Costa et al., 2019; Nwagu et al., 2021; Remonatto et al., 2022).

Immobilization can be divided into four main methods: adsorption, entrapment, covalent linking, and crosslinking. Entrapment is an irreversible, inexpensive, and simple technique that embeds enzymes in a polymer network. This method prevents enzyme aggregation and leaching and improves stability. Furthermore, entrapment in a gel matrix is a mild process that provides the necessary conditions for the enzyme to retain its optimal structure. However, a disadvantage of such a method is that the gel wall represents a barrier to the mass transfer of substrates from the bulk medium to active sites and prevents the transfer of products in the opposite direction (Bolivar et al., 2022; Imam et al., 2021; Rafiee and Rezaee, 2021).

In addition to the advantages and disadvantages reported above, another important point is that the immobilization process may affect enzyme kinetics, mainly enzyme–substrate affinity (K_m) and maximum velocity (V_{max}). These effects usually stem from changes in enzyme flexibility, diffusional limitations, and the formation of the Nernst diffusion layer (Agrawal et al., 2016; Almeida et al., 2021a, 2021b). However, the occurrence and extent of such changes in enzyme kinetics depend on the type of enzyme and immobilization technique.

Riley et al. (1997) used a computational model to evaluate oxygen migration through cells immobilized in 0.5, 1, and 2 mm beads. The results showed that oxygen penetrated to a maximum depth of about 0.4 mm and that smaller beads contained a higher density of viable cells, had higher cell viability, and produced more antibodies per unit volume, which may be associated with reduced mass transfer problems. Liu (2020), in a theoretical study, described that the particle size effect follows the same trend seen in solid catalyzed systems: smaller bead sizes lead to higher mass transfer rate and efficiency. Alloue et al. (2008) studied the immobilization of lipase in alginate beads by extrusion dripping and obtained immobilization yields of 36.1% and 39% for beads measuring 2.43 and 1.41 mm, respectively. The authors stated that, as expected, the activity of entrapped lipase decreased as bead size increased.

Extrusion dripping, the method traditionally used for bead production, produces large particles measuring about 2 mm. Jet cutting has been proposed as a tool to combine the advantages of gel entrapment with the possibility of producing smaller beads. Jet cutting involves pumping a solution through a nozzle at a high flow rate in order to produce a continuous jet. A snipping tool placed at the outlet of the nozzle cuts the jet, leading to a reduction in bead size (Prüße et al., 1998b; Prüße et al., 2002; Paulo et al., 2017).

Prüße et al. (1998a) produced 0.2 mm alginate beads using high rotation (2000 rpm). Paulo et al. (2017) obtained jet-cut alginate beads measuring only 1.1 (900 rpm) and 1.5 mm (600 rpm), whereas those produced by dripping measured between 2.2 and 4.6 mm. The authors noted that an increase in rotation speed led to a reduction in bead size.

The process of particle formation in both techniques is based on the ionic replacement of the sodium of sodium alginate by calcium ions (Ca^{2+}) from calcium chloride, as widely reported in the literature (Carvalho et al., 2021; de Moura et al., 2018; de Souza et al., 2022). The replacement mechanism is nonselective, involving carboxyl and hydroxyl groups of the polymeric chain in such a manner that an interleaved "egg-box" structure is created (Souza et al., 2022; Kabir et al., 2020; Silverio et al., 2018). According to Cao et al. (2020), the formation process can be divided into three distinct and successive steps: (i) formation of monocomplexes between Ca^{2+} and guluronic acid units in a single alginate chain, (ii) formation of egg-box dimers by the pairing of monocomplexes, and (iii) formation of multimers through the lateral crosslinking of egg-box dimers.

The high yield and small bead size afforded by jet cutting suggest good potential for enzyme entrapment. However, jet cutting is still a new technology, and more studies are needed to understand phenomena occurring during bead formation. No study has yet assessed the use of jet cutting for lipase immobilization. To fill this gap, this study aimed to produce a novel entrapped lipase biocatalyst by the jet cutting technique and compare it with a drip-formed biocatalyst.

2. Material and methods

2.1. Chemicals

Lipase Eversa® Transform 2.0 (lipase from *Thermomyces lanuginosus* expressed in *Aspergillus oryzae*, Novozymes S/A), *p*-nitrophenyl palmitate (pNPP), *p*-nitrophenyl (pNP), and fluorescein isothiocyanate isomer I (FITC) were purchased from Sigma–Aldrich (St. Louis, MO, USA). Sodium alginate (Manugel GMB, MW = 170–240 kDa; mannuronic acid/galacturonic acid ratio ≅ 40:60) was kindly donated by DuPont Brasil (Cotia, SP, Brazil).

2.2. Influence of flow rate on jet-cut beads

The effects of jet flow rate (18.46 ± 0.28, 36.44 ± 0.51, 46.93 ± 0.40, and 52 ± 1.33 mL min^{-1}) on mass yield and bead size were studied. Sodium alginate solution (2% w/v) was pumped by a peristaltic pump (MasterFlex®, Cole-Parmer, Chicago) through silicone tubing (4 mm i.d., 51 mm wall thickness) to a double-jacketed fluid atomizing nozzle (1 mm i.d.). Drops were allowed to fall into a 200 mM solution of calcium chloride ($CaCl_2$). The rotation of the cutting tool was set at 1200 rpm, the distance between the nozzle and the cutting tool was 1 cm, and the distance between the cutting tool and the calcium chloride solution was 4 cm (Paulo et al., 2017). Mass yield was calculated as the ratio of the initial weight of the sodium alginate solution to the weight of drained beads.

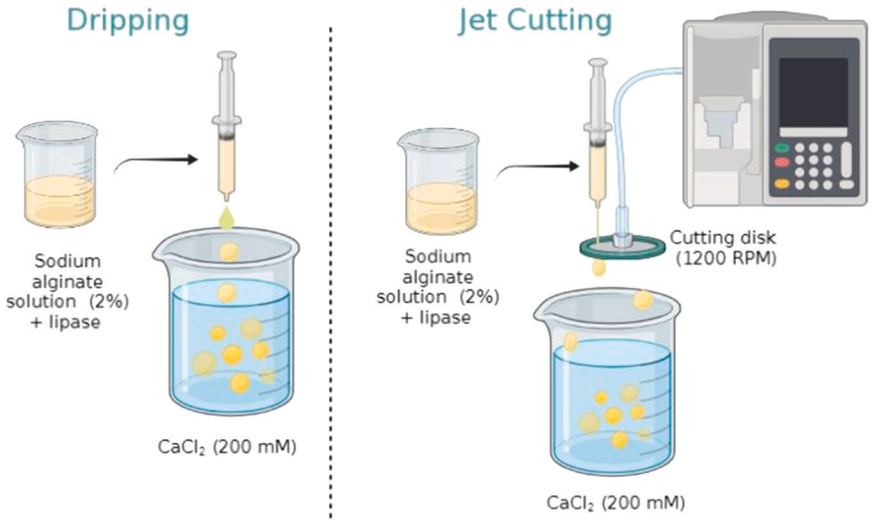

Fig. 1 – Illustrative diagram of dripping and jet cutting immobilization techniques.

2.3. *Lipase immobilization by dripping and jet cutting methods*

The two lipase immobilization processes are depicted in Fig. 1. First, Eversa® Transform 2.0 was added to 2% (v/v) sodium alginate at a ratio of 5 mL of enzyme to 100 mL of polymer solution. Then, the resulting solution was stirred for 10 min using a magnetic stirrer. Afterward, the solution was dripped into a 200 mM $CaCl_2$ solution. The flow rate was 2.72 ± 0.10 mL min^{-1} for dripping and 52 ± 1.33 mL min^{-1} for jet cutting. Beads were left to rest for 15 min in $CaCl_2$ solution, filtered through a sieve, and washed with distilled water.

2.4. *Characterization of beads produced by jet cutting and dripping methods*

Identification of the functional groups was performed by Fourier transform infrared spectroscopy (FTIR). FTIR spectra were recorded at a resolution of 4 cm^{-1} in the wavenumber range of 400–4000 cm^{-1} using an FTIR ATR Cary 630 spectrometer (Agilent, Bayan Lepas, Malaysia) equipped with MicroLab PC and Resolution PRO software (version 5.1.0.8). Before the analysis, samples were freeze-dried (Enterprise, Terroni, São Paulo, Brazil) for 24 h. The same procedure was carried out for Brunauer–Emmett–Teller (BET), apparent and true density, and scanning electron microscopy (SEM) analyses.

Specific surface area was determined by N_2 physisorption (Anton Paar, Quantachrome NOVA 1200e, Germany) at 77 K and estimated by the BET method. Apparent density and pore size distribution were determined by mercury porosimetry (Micromeritics Instrument Corporation, AutoPore IV 9500, Norcross, Georgia, USA) under low (0.03–2.41 bar) and high (2.41–4136.85 bar) pressure. True density was determined by helium gas pycnometry (Micromeritics Instrument Corporation, AccuPyc II 1340, Norcross, Georgia, USA).

The mean diameter of beads was determined by laser diffraction using an LV 950-V2 equipment (Horiba, Kyoto, Japan) according to a wet method with 99.5% dispersion. Mean bead sizes are expressed as mean volume diameters ($D_{[3,4]}$). The polydispersity of small beads was estimated by the span index, calculated according to Eq. (1).

$$\text{Span} = (D_{[0.9]} - D_{[0.1]})/D_{[0.5]} \quad (1)$$

where $D_{[0.1]}$, $D_{[0.5]}$, and $D_{[0.9]}$ are the diameters at 10%, 50%, and 90% of the cumulative size distribution curve, respectively.

Wet particles were examined under a Nikon optical microscope (AZ100, Tokyo, Japan) at 4 × magnification and analyzed using Zen 2.6 software. SEM images were acquired using a scanning electron microscope (Hitachi TM4000Plus) equipped with TM4000 software. The microscope was operated at high vacuum conditions and an accelerating voltage of 15 kV. All samples were sputtered with gold before analysis.

Confocal laser scanning microscopy (CLSM) was carried out according to Zhang et al. (2016), using a confocal microscope (Leica, TCS SP5 II, Leica Microsystems, Wetzlar, Germany) and oil-immersion objective lenses ranging from 20 × to 100 × . Excitation and emission wavelengths were 488 and 515 nm, respectively. Lipase was stained by mixing 2 mL of sample before immobilization with 0.1 mL of FITC solution (2 mg of FITC per 1 mL of dimethyl sulfoxide). The resulting solution (lipase + FITC) was kept at room temperature under agitation (1000 rpm) for 1 h and then stored under refrigeration for 7 h without agitation. After this period, excess FITC was removed by centrifugation using a Falcon tube with a 10 kDa membrane. Lipase was added to sodium alginate solution, and bead production was carried out as described above.

2.5. *Immobilization parameters*

Immobilization yield and recovered enzyme activity were calculated based on the following equations (Eqs. 2 and 3) (Boudrant et al., 2020; Sheldon and van Pelt, 2013):

$$Y_{im} = \left(\frac{EA_{free} - EA_{supernatant}}{EA_{free}}\right) \times 100 \quad (2)$$

$$RA = \left(\frac{EA_{derivative}}{EA_{free} - EA_{supernatant}}\right) \times 100 \quad (3)$$

where Y_{im} is the immobilization yield (%), EA_{free} the specific activity of the free enzyme (U g^{-1}), $EA_{supernatant}$ the specific activity of the supernatant (U g^{-1}), RA the recovered enzyme

Table 1 – Coded and real values used in the central composite rotatable design to study the effect of pH and temperature on lipase hydrolytic activity.

Variable	Code	Level				
		−1.41	−1	0	+1	+1.41
pH	x_1	5	6	8	10	11
Temperature (°C)	x_2	30	36	50	64	70

activity (U g^{-1}), and $EA_{derivative}$ the specific activity of the immobilized derivative (U g^{-1}).

2.6. Effect of pH and temperature on lipase activity

A central composite rotatable design was used to simultaneously study the effect of pH and temperature on lipase activity (Table 1). Experiments were arranged as a 2^2 full factorial with 4 axial points and 3 repetitions of the center point, totaling 11 runs (Rodrigues and Iemma, 2014).

pH and temperature effects were analyzed at $p < 0.1$ using Protimiza experimental design software (https://experimental-design.protimiza.com.br/), which was also used to calculate factor levels and create the design matrix (Rodrigues and Iemma, 2014).

2.7. Enzyme activity and protein concentration

Protein concentration was determined according to the Dumas method (Dumas, 1831). Quantification was performed against a standard curve of rice flour solution using a nitrogen analyzer (NDA 701, Velp Scientifica, Italy).

Lipase hydrolytic activity was determined by measuring the hydrolysis of pNPP to pNP (Bresolin et al., 2020; Chiou and Wu, 2004). First, 500 µL of substrate (0.005% pNPP in ethanol) was added to 440 µL of phosphate buffer (1 M, pH 7.0). Then, 60 µL or 60 mg of free or immobilized lipase was added to start the reaction. After incubation at 35 °C for 5 min, the reaction was stopped by adding 1000 µL of 0.5 M sodium hydroxide (pH 13). The mixture was centrifuged at 1000 rpm for 10 min. Finally, the absorbance of a 1000 µL aliquot was measured using a spectrophotometer (Genesys 20, Thermo Fisher Scientific). Quantification was performed using a standard curve of pNP. One unit of enzyme activity (U) was defined as the amount of enzyme needed to release 1 µmol of pNP in 1 min. All experiments were performed in duplicate.

3. Results and discussion

3.1. Influence of flow rate on the production of jet-cut beads

The results of the effect of different flow rates on jet-cut beads are shown in Table 2. There were no statically significant differences in mass yield or bead size between flow rates; all mass yields were greater than 65%.

The variation in bead size as a function of flow rate observed in our study corroborates the results found in the literature. Prüße et al. (1998a) produced 0.2 mm alginate beads using high rotation (2000 rpm), and Paulo et al. (2017) produced alginate beads measuring 1.1 mm by jet cutting at 900 rpm and 1.5 mm by jet cutting at 600 rpm. As we used an intermediate rotation (1200 rpm), it was expected to obtain intermediate sizes, given that an increase in rotation speed results in a reduction in bead size, as previously reported (Paulo et al. 2017).

Polydispersity values lower than 1.0 were obtained under all flow rate conditions. The values were similar to those reported by (Paulo et al. 2017). A flow rate of 52 mL min^{-1} was used for lipase immobilization in further experiments because it provided the highest yield.

3.2. Physical characterization of beads

Mass yield was influenced by bead production technique. Whereas dripping afforded a mass yield of 76.19% ± 2.03%, jet cutting afforded a lower value (52.24% ± 6.46%). The lower mass yield obtained by jet cutting is due to the small size of the collecting recipient (Paulo et al., 2017), which favors collision of the jet with recipient walls. A larger collecting recipient is recommended, as it may provide a higher yield. Jet cutting (24.60 ± 3.05 g min^{-1}) provided an 18.82 times higher yield than extrusion dripping (1.66 ± 0.01 g min^{-1}). High yields are crucial for industrial application.

The physical characteristics of beads obtained by both techniques are shown in Table 3. The mean diameter of lipase-loaded jet-cut beads (803.36 ± 16.93 µm) was 3 times smaller than that of beads obtained by extrusion dripping (2459.98 ± 15.64 µm). Both materials showed low polydispersity and monomodal distribution. Moura et al. (2018) used a feed rate of 11.5 mL min^{-1} and obtained beads ranging in size from 841.6 to 1169.22 µm and in span from 0.55 to 0.59. The authors used an encapsulating equipment that produces beads whose final size depends on the vibration frequency (100–2200 Hz) and electrode tension (400–2000 V) used to break the jet. The size of beads produced by jet cutting is

Table 2 – Mass yield, size, and span of beads as a function of jet flow rate.

Parameter	Flow rate			
	A	B	C	D
Mass yield (%)	70.65^{a} ± 2.40	68.00^{a} ± 4.82	72.27^{a} ± 2.47	73.22^{a} ± 2.54
$D_{[3,4]}$ (µm)	782.73^{a} ± 88.40	780.52^{a} ± 57.65	770.24^{a} ± 23.90	$840,82^{a}$ ± 32.45
$D_{[10]}$ (µm)	389.08^{b} ± 19.86	432.95^{ab} ± 15.12	447.97^{a} ± 28.45	486.20^{a} ± 28.77
$D_{[50]}$ (µm)	807.83^{a} ± 55.83	786.71^{a} ± 44.67	782.25^{a} ± 20.06	835.95^{a} ± 25.65
$D_{[90]}$ (µm)	1223.59^{a} ± 199.22	1102.43^{a} ± 128.64	1067.49^{a} ± 34.83	1189.95^{a} ± 55.83
Span	0.98^{a} ± 0.13	0.84^{a} ± 0.13	0.79^{a} ± 0.02	0.84^{a} ± 0.04

A, 18.46 ± 0.28 mL min^{-1}; B, 36.44 ± 0.51 mL min^{-1}; C, 46.93 ± 0.40 mL min^{-1}; D, 52 ± 1.33 mL min^{-1}. Means in the same row followed by the same letter do not differ significantly from each other (Tukey's test, $p < 0.05$).

Table 3 – Physical properties of lipase-loaded beads prepared by jet cutting or extrusion dripping, as assessed by Brunauer–Emmett–Teller (BET) surface area measurement, mercury porosimetry ($\rho_{apparent}$), and helium gas pycnometry (ρ_{true}).

Parameters	Jet cutting	Dripping
$D_{[3,4]}$ (μm)	803.36 ± 16.93	2459.98 ± 15.64
$D_{[10]}$ (μm)	487.83 ± 26.87	1885.17 ± 18.78
$D_{[50]}$ (μm)	804.16 ± 11.55	2475.82 ± 11.18
$D_{[90]}$ (μm)	1119.93 ± 27.32	3000.09 ± 6.81
Span	0.79 ± 0.04	0.45 ± 0.01
BET surface area ($m^2\ g^{-1}$)	5.46	3.13
$\rho_{apparent}$ ($g\ cm^{-3}$)	0.43	1.41
ρ_{true} ($g\ cm^{-3}$)*	1.81	1.80
Porosity (%)	76.24	21.65

*Unloaded beads.

similar to that of beads produced by encapsulation; however, with jet cutting, it is possible to achieve a 4.52 times higher yield, and it is not required to apply vibration frequency or electrode tension.

The low polydispersity of jet-cut beads can be explained by the fact that high feed capacity imposes greater kinetic energy on droplet generation, leading to uneven disintegration of jet liquid into individual droplets, and, consequently, a polydisperse size distribution. Given the complexity of the bead formation technique, encompassing opening size, fluid pressure, fluid viscosity, cut, and tangential displacement, it is expected to obtain a more disperse system. A similar behavior is obtained with spray drying (Wu et al., 2007), in which several forces act to break droplets in the atomizer.

As a consequence of their smaller size, jet-cut beads showed higher surface area ($5.46\ m^2\ g^{-1}$) than drip-formed beads ($3.13\ m^2\ g^{-1}$). The specific surface area of alginate beads was similar to that of beads obtained by dripping in the study of Mai et al. (2013) ($2.58\ m^2\ g^{-1}$). Higher surface area is of utmost importance to improve mass transfer in biocatalyst applications.

Increasing the specific surface area of gel beads would facilitate mass transfer during enzymatic reactions. Khoo and Ting (2001) observed faster metal uptake kinetics for fungi-loaded polyvinyl alcohol beads than for fungi-loaded alginate beads and attributed this difference to the larger BET area of the former ($48.1\ m^2\ g^{-1}$) compared with that of the latter ($6.25\ m^2\ g^{-1}$).

Jet-cut beads had a $\rho_{apparent}$ of $0.43\ g\ cm^{-3}$ and a ρ_{true} of $1.81\ g\ cm^{-3}$, whereas beads obtained by extrusion dripping exhibited $\rho_{apparent}$ and ρ_{true} values of $1.41\ g\ cm^{-3}$ and $1.80\ g\ cm^{-3}$, respectively. According to Costa et al. (2021), $\rho_{apparent}$ is calculated based on the relationship between mass and total volume of the solid, that is, the real volume of the adsorbent added to the volume occupied by Hg filling the pores of the solid. ρ_{true} is obtained by the ratio of mass to real volume, without considering empty pore volume. Thus, in this case, the higher density of drip beads might be associated with the fact that larger beads occupy a greater total volume, thereby increasing the $\rho_{apparent}$ value.

The porosity of jet-cut beads was 3.60 times greater than that of drip-formed beads. Deze et al. (2012) studied alginate aerogel beads and found a beneficial effect of porosity on diffusion. Thus, it is believed that high porosity may be associated with better substrate and product diffusion rates.

The N_2 isotherms obtained by BET area analysis were classified as type II (Fig. 2), characteristic of non-porous or macroporous adsorbents. Structures are considered macroporous when pores have diameters greater than 50 nm, according to the International Union of Pure and Applied Chemistry (IUPAC) (Thommes et al., 2015). These results corroborate those of pore size distribution by mercury porosimetry, which indicated that bead pores were larger than 50 nm, being classified as macroporous. Given that both types of beads were macroporous, it is believed that size reduction did not influence the diffusion rate of sodium alginate crosslinking.

Larger pores provide less resistance to mass transfer but may make it difficult for some substances to be entrapped (Kazan et al., 2017). Costa et al. (2021) produced beads from sericin/alginate/polyvinyl alcohol and observed a large number of macropores, as found here. Silva et al. (2021) prepared sericin/alginate beads crosslinked by polyethylene glycol diglycidyl ether via dripping and found the beads to be macroporous.

3.3. *FTIR and image analysis*

Free lipase and beads were characterized by FTIR (Fig. 3). The presence of peaks at 3400–3200 cm^{-1} in the spectrum of free lipase is attributed to O–H stretching and asymmetric stretching of the primary amide NH_2. It should be noted that the peak is intensified because of the presence of water and sorbitol in the enzyme extract. The peak at 1650 cm^{-1} is associated with the amide II band and the peak at 1400–1200 cm^{-1} is due to the amide III mode (Bresolin et al., 2019; Collins et al., 2011; Foresti et al., 2010).

All beads showed a peak in the 3600–3000 cm^{-1} region, which might be related to stretching vibrations of alginate O–H bonds (Daemi and Barikani, 2012). Although loaded beads contained small amounts of lipase, some changes were observed in their spectra compared with that of unloaded beads, mainly in the 1000–800 cm^{-1} and 1300–1200 cm^{-1} regions.

Bead morphology is depicted in Fig. 4 and S1 (Supplementary Material). Although both beads were spherical, drip-formed beads appeared to be more spherical than jet-cut beads. Paulo et al. (2017) found that an increase in jet cutter speed leads to a reduction in bead size but not to a change in morphology (beads continue to be spherical). The spherical structure of beads is related to surface tension forces, which should be sufficient to overcome impact and drag effects during the fall (Paulo et al., 2017; Prüße et al., 1998a).

As shown in SEM micrographs, beads produced by extrusion dripping (Fig. 4a1–b3) were larger than those produced by jet cutting (Fig. 4c1–d3), in agreement with size measurements. Bead shape was not influenced by production technique. By either preparation method, unloaded beads (Fig. 4a1–a3 and c1–c3) had a smooth, crack-free surface, whereas loaded beads exhibited roughness and cracks, confirming the presence of lipase. Similar results were found

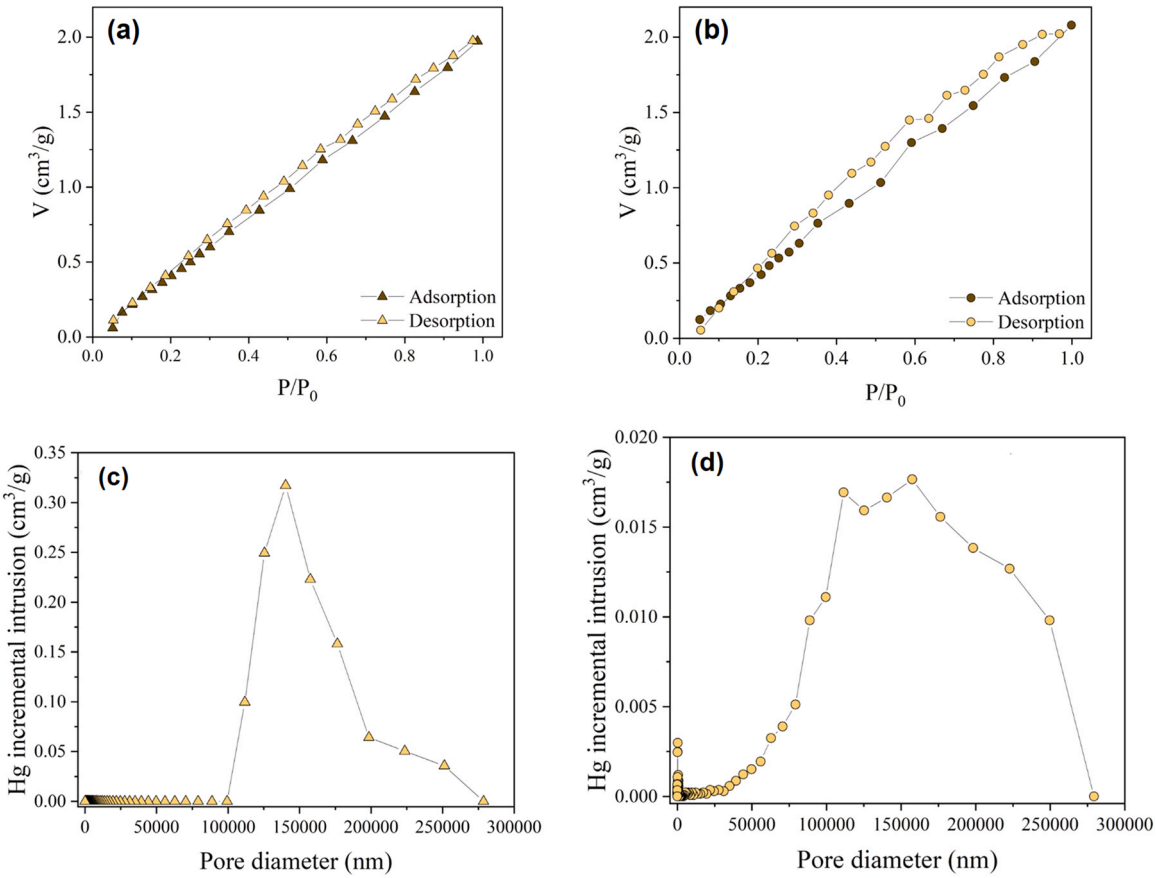

Fig. 2 – N_2 adsorption/desorption isotherms determined by Brunauer–Emmett–Teller surface area analysis (a, b) and pore size distribution determined by mercury porosimetry (c, d) of beads obtained by jet cutting (a and c) or extrusion dripping (b and d).

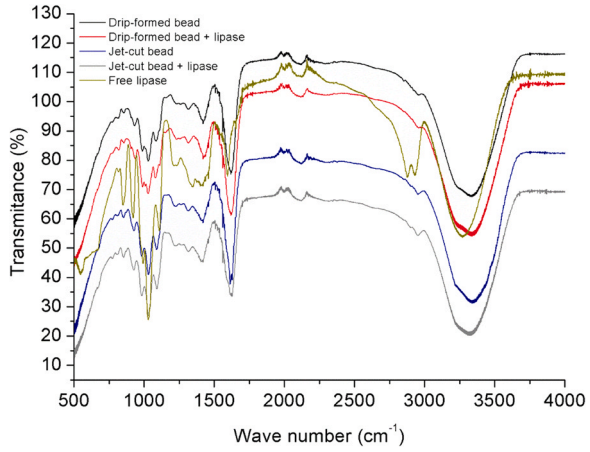

Fig. 3 – FTIR spectra of free lipase, lipase-loaded and unloaded beads produced by extrusion dripping, and lipase-loaded and unloaded beads produced by jet cutting.

by Aharwar and Parihar (2021), Facin et al. (2018), and Kumar et al. (2017).

CLSM was used to confirm the presence of lipase in beads. According to Amirkhani et al. (2016) and Ghide et al. (2022), this technique can be used to visualize the distribution of lipase on dispersed and non-dispersed supports, as well as to evaluate diffusion restrictions within materials. CLSM images (Fig. 5) support SEM results, confirming the presence of lipase in beads (intense green points). It is possible to observe the distribution of lipase throughout beads, with similar patterns in both types of beads. The low density of green points is due to the low content of lipase used for immobilization. The presence of enzyme-free spaces (weak green) suggests the possibility of using higher enzyme loadings.

3.4. *Immobilization parameters*

An immobilization yield of 100% was obtained with both techniques, as lipase activity was not identified in the $CaCl_2$ solution. Pereira et al. (2018) obtained immobilization yields of 91.76–99.77% using *Yarrowia lipolytica* lipase. Drip-formed and jet-cut beads had recovered activities of 28.26% ± 1.19% and 30.13% ± 1.99%, respectively. It is known that enzyme activity may be affected by several factors during immobilization, including enzyme content (Yagar and Balkan, 2017). We believe that, because of the low amount of enzyme used, it was possible to achieve full entrapment.

The low values of recovered activity might be due to mass transfer problems. Imam et al. (2021) reported that mass transfer limitations are a drawback of the entrapment method; the material must be designed with appropriate pore size and matrix properties.

3.5. *Effect of pH and temperature on lipase hydrolytic activity*

On the basis of the previous experimental design, we carried out 11 runs in random order to study the effect of two

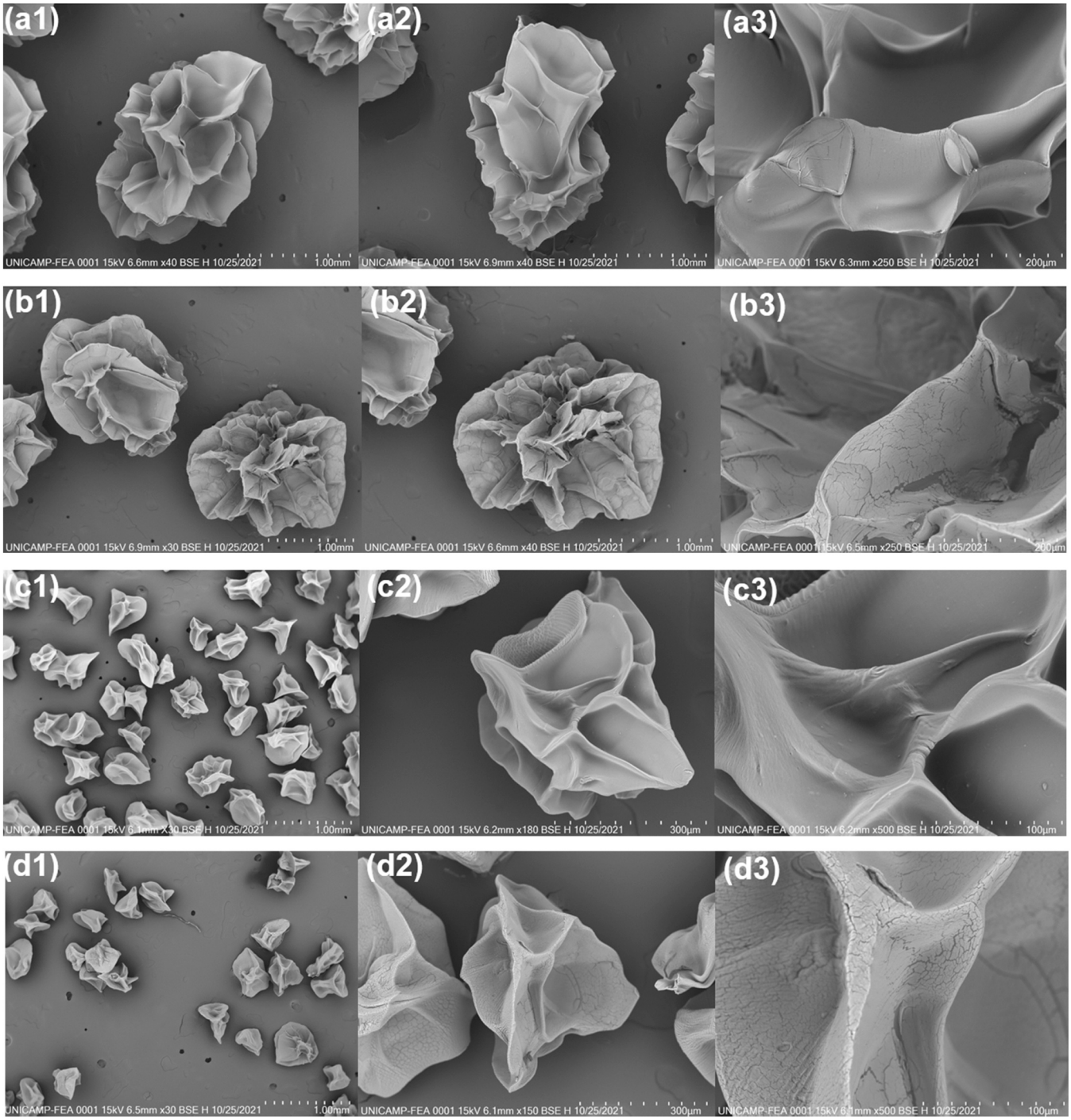

Fig. 4 – Surface topography of calcium alginate beads by scanning electron microscopy. a1–a3, unloaded beads obtained by extrusion dripping; b1–b3, lipase-loaded beads obtained by extrusion dripping; c1–c3, unloaded beads obtained by jet cutting; and d1–d3, lipase-loaded beads obtained by jet cutting.

variables on enzyme activity. Table 4 shows the coded and real values of independent variables (factors) and the enzyme activity (response) obtained in each run. Table S3 (Supplementary Material) presents the predicted and relative errors of enzyme activity.

As described in Table 4, the highest enzyme activities were obtained at alkaline pH (pH 10 and 11). High hydrolytic activities for free lipase were observed under high pH combined with low temperature conditions. Immobilized lipases (entrapped in drip-formed and jet-cut beads) showed excellent results at high temperatures and pH values, demonstrating that immobilization provided an increase in the useful temperature range. A similar behavior was reported by Simón-Herrero et al. (2019) in studying the immobilization of laccase on polyimide aerogels.

Analysis of the effects of parameters on hydrolytic activity was carried out considering regression coefficients and p-values ($p < 0.1$), as shown in Table S1 (Supplementary Material). Temperature was significant for free lipase and lipase entrapped in drip-formed beads but not for lipase immobilized on jet-cut beads. The pH was significant for all biocatalysts. Three coded models containing the significant coefficients were generated, as shown in Eq. (4) (free lipase), (5) (drip-formed beads), and (6) (jet-cut beads).

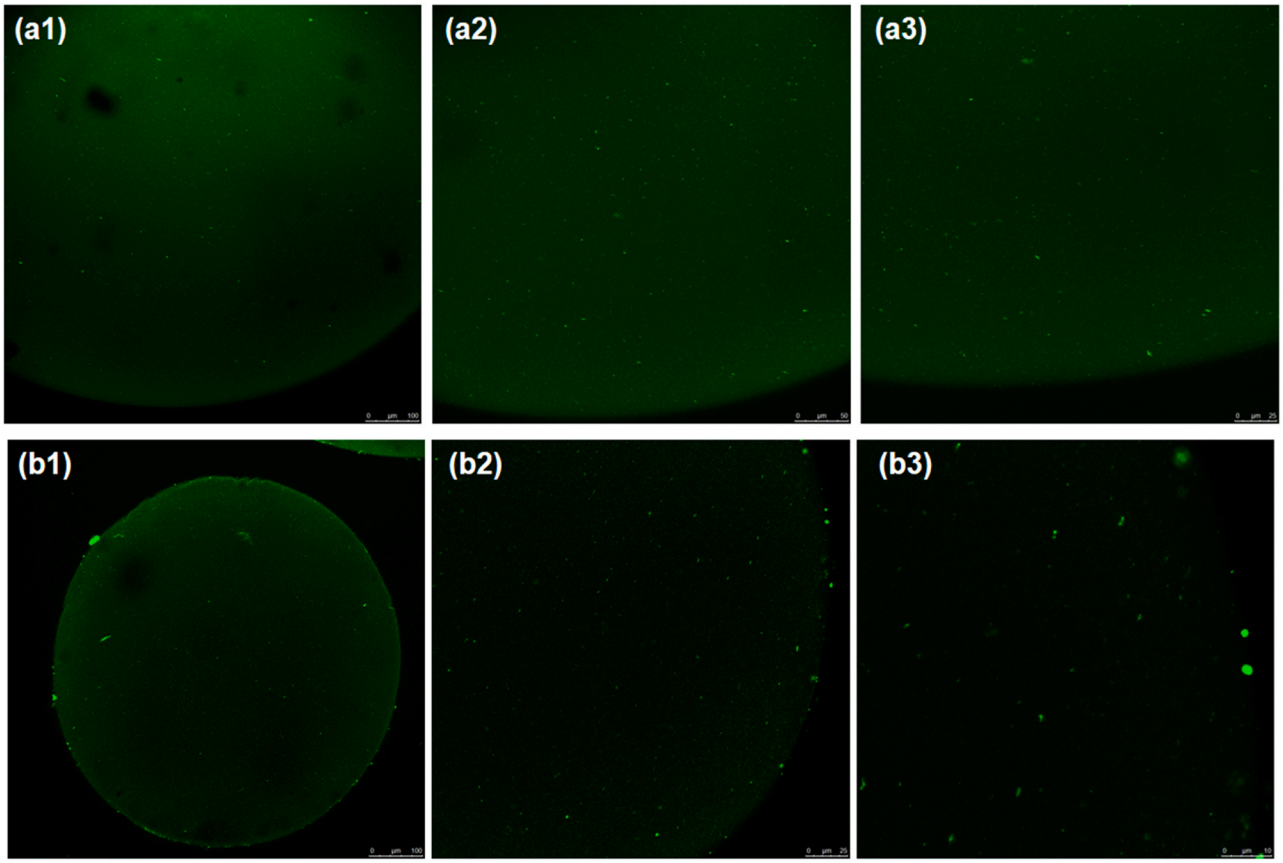

Fig. 5 – Confocal laser scanning microscopy images of calcium alginate beads (20 ×, 43 ×, and 60 × magnification). a1–a3, beads obtained by extrusion dripping; b1–b3, beads obtained by jet cutting.

$$Y_1 = 1077{\cdot}40 + 1830{\cdot}20x_1^2 - 1314{\cdot}09x_2 + 1312{\cdot}76x_2^2 - 3192{\cdot}17x_1x_2 \quad (4)$$

$$Y_2 = 328{\cdot}80 + 333{\cdot}40x_1 + 240{\cdot}93x_1^2 + 67{\cdot}47x_2 - 95{\cdot}16x_2^2 + 150{\cdot}13x_1x_2 \quad (5)$$

$$Y_3 = 333{\cdot}73 + 754{\cdot}52x_1 + 764{\cdot}04x_1^2 \quad (6)$$

Analysis of variance (Supplementary Material) showed that the models were valid, with R^2 values of 91.22% (free lipase), 99.33% (drip-formed beads), and 97.00% (jet-cut beads). *F*-values were higher than *F*-critical values (Rodrigues and Iemma, 2014). The contour plots of regression equations are shown in Fig. 6.

Fig. 6a shows that free lipase had a better activity in the pH range of 9–11 and low temperatures (30–40 °C). A similar behavior was observed by Miranda et al. (2020), who found increased activity at pH 5–10 and temperatures of 10–70 °C for the same lipase. Free lipase reached a hydrolytic activity of 15,000 U g^{-1} (Fig. 6a), with optimal activity in the pH range of 9–11 and low temperatures (30–40 °C).

Immobilization via extrusion dripping (Fig. 6b) afforded activities of up to 1500 U g^{-1}. The best results were observed in the temperature range of 40–70 °C at alkaline pH. pH and

Table 4 – Hydrolytic activity of free lipase and lipase immobilized on beads obtained by extrusion dripping or jet cutting, as assessed at different pH values and temperatures.

Run	pH (x_1)	Temperature, °C (x_2)	Hydrolytic activity (U g^{-1})		
			Free lipase	Drip-formed beads	Jet-cut beads
1	6 (–1)	36 (–1)	2932.63	216.22	308.88
2	10 (1)	36 (–1)	8522.19	548.97	1775.96
3	6 (–1)	64 (1)	7456.61	64.86	106.35
4	10 (1)	64 (1)	277.50	998.13	1568.49
5	5 (–1.41)	50 (0)	5364.49	332.81	921.18
6	11 (1.41)	50 (0)	2957.38	1323.59	3118.12
7	8 (0)	30 (–1.41)	5527.37	70.46	230.07
8	8 (0)	70 (1.41)	724.71	241.57	460.13
9 (C)	8 (0)	50 (0)	1009.92	281.83	431.38
10 (C)	8 (0)	50 (0)	946.63	322.09	402.62
11 (C)	8 (0)	50 (0)	1275.65	382.49	460.13

C, center point.

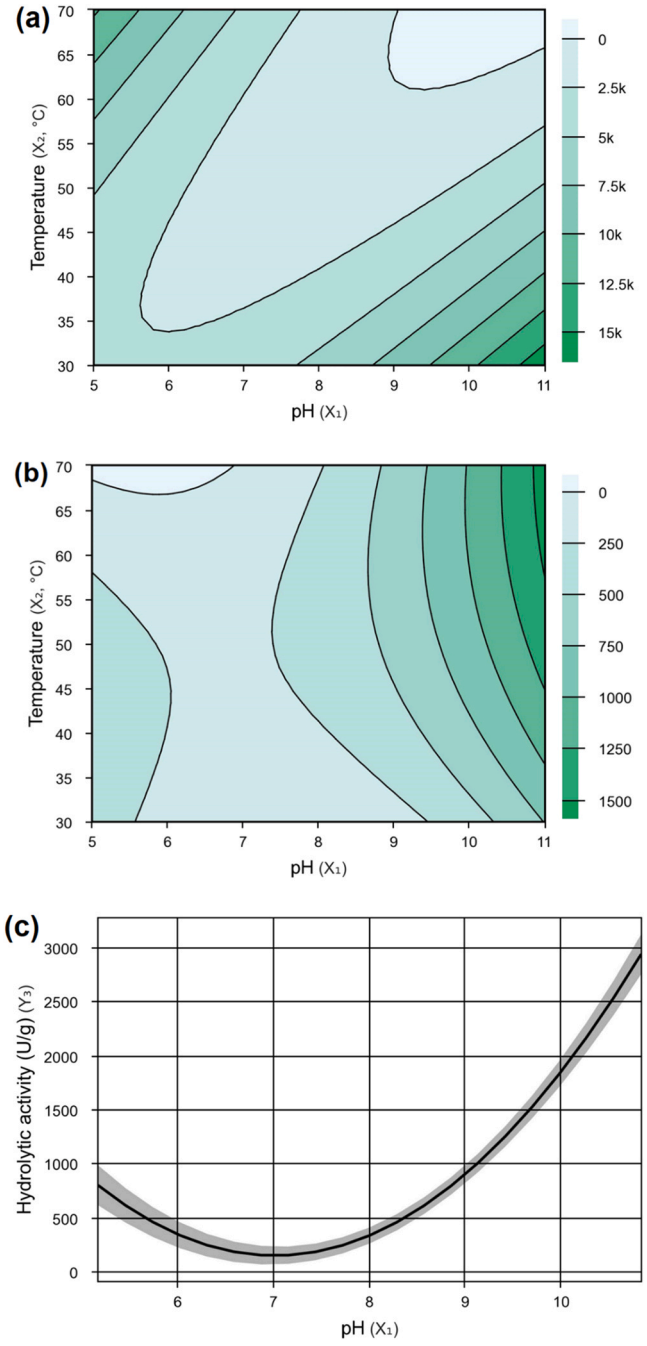

Fig. 6 – Contour plots of (a) free lipase and lipase immobilized on beads produced by (b) extrusion dripping and (c) jet cutting.

temperature exerted significant effects on the enzymatic activity of lipase immobilized on drip-formed beads, with greater influence of pH (Fig. 6b). It is believed that temperature had a slightly positive effect, as mass transfer increases at higher temperatures, facilitating contact between substrate and active sites.

As depicted in Fig. 6c, enzymes immobilized by jet cutting had higher activity (up to 3000 U g^{-1}) than lipase immobilized by dripping at any temperature in the studied range. At pH 10.5 and 50 °C, jet-cut beads had higher activity (2531 U g^{-1}) than drip-formed beads (1131 U g^{-1}). Thus, about half of the amount of jet-cut beads can be used to achieve a similar hydrolytic activity as drip-formed beads. The non-significant effect of temperature on enzyme activity might be associated with the fact that lipases immobilized on jet-cut beads were protected from high temperatures. Furthermore, jet-cut beads showed higher porosity than drip-formed beads, a characteristic that facilitates access to the substrate.

4. Conclusion

Immobilization of Eversa® Transform 2.0 via jet cutting was found to be an interesting strategy compared with extrusion dripping. Jet cutting allowed obtaining smaller beads and higher yields than dripping. Furthermore, jet cutting provided an increase in mass transfer rate and superficial area, as well as higher lipase hydrolytic activity, compared with dripping. Future studies should focus on improving the break of droplets by jet cutting. Nevertheless, our results indicated the potential of this technique for lipase immobilization.

Declaration of Competing Interest

The authors declare that they have no known competing financial interests or personal relationships that could have appeared to influence the work reported in this paper.

Acknowledgments

This study was supported by the São Paulo Research Foundation (FAPESP, grant No. 2019-03399-8), the Brazilian National Council for Scientific and Technological Development (CNPq), and the Coordenação de Aperfeiçoamento de Pessoal de Nível Superior (CAPES, Finance Code 001). The authors are grateful to Adilson Brandão, MSc (LRAC-UNICAMP), for assisting with SEM analysis, to Dr. Beatriz Travália for assisting with data interpretation, and to the team of the Central Laboratory of High-Performance Technologies in Life Sciences (LaCTAD).

Appendix A. Supporting information

Supplementary data associated with this article can be found in the online version at doi:10.1016/j.fbp.2022.12.001.

References

Agrawal, R., Verma, A.K., Satlewal, A., 2016. Application of nanoparticle-immobilized thermostable β -glucosidase for improving the sugarcane juice properties. Innov. Food Sci. Emerg. Technol. 33, 472–482. https://doi.org/10.1016/j.ifset.2015.11.024

Aharwar, A., Parihar, D.K., 2021. Talaromyces verruculosus tannase immobilization, characterization, and application in tea infusion treatment. Biomass Convers. Biorefinery. https://doi.org/10.1007/s13399-020-01162-6

Alloue, W.A.M., Destain, J., El Medjoub, T., Ghalfi, H., Kabran, P., Thonart, P., 2008. Comparison of yarrowia lipolytica lipase immobilization yield of entrapment, adsorption, and covalent bond techniques. Appl. Biochem. Biotechnol. 150 (1), 51–63. https://doi.org/10.1007/s12010-008-8148-9

Almeida, Francisco L.C., Prata, A.S., Forte, M.B.S., 2021. Enzyme immobilization: what have we learned in the past five years. Biofuels Bioprod. Bioref. https://doi.org/10.1002/bbb.2313

Almeida, Francisco Lucas Chaves, Castro, M.P.J., Travália, B.M., Forte, M.B.S., 2021. Trends in lipase immobilization: Bibliometric review and patent analysis. Process Biochem. 110, 303–321. https://doi.org/10.1016/j.procbio.2021.10.012

Amirkhani, L., Moghaddas, J., Jafarizadeh-Malmiri, H., 2016. Candida rugosa lipase immobilization on magnetic silica

aerogel nanodispersion. RSC Adv. 6 (15), 12676–12687. https://doi.org/10.1039/C5RA24441B
Badoei-dalfard, A., Tahami, A., Karami, Z., 2022. Lipase immobilization on glutaraldehyde activated graphene oxide/chitosan/cellulose acetate electrospun nanofibrous membranes and its application on the synthesis of benzyl acetate. Colloids Surf. B: Biointerfaces 209, 112151. https://doi.org/10.1016/j.colsurfb.2021.112151
Bolivar, J.M., Woodley, J.M., Fernandez-lafuente, R., 2022. Is enzyme immobilization a mature discipline ? Some critical considerations to capitalize on the benefits of immobilization. Chem. Soc. Rev. 6251–6290. https://doi.org/10.1039/d2cs00083k
Boudrant, J., Woodley, J.M., Fernandez-Lafuente, R., 2020. Parameters necessary to define an immobilized enzyme preparation. Process Biochem. 90, 66–80. https://doi.org/10.1016/j.procbio.2019.11.026
Bresolin, D., Estrella, A.S., da Silva, J.R.P., Valério, A., Sayer, C., de Araújo, P.H.H., de Oliveira, D., 2019. Synthesis of a green polyurethane foam from a biopolyol obtained by enzymatic glycerolysis and its use for immobilization of lipase NS-40116. Bioprocess Biosyst. Eng. 42 (2), 213–222. https://doi.org/10.1007/s00449-018-2026-9
Bresolin, D., Hawerroth, B., de Oliveira Romera, C., Sayer, C., de Araújo, P.H.H., de Oliveira, D., 2020. Immobilization of lipase Eversa Transform 2.0 on poly(urea–urethane) nanoparticles obtained using a biopolyol from enzymatic glycerolysis. Bioprocess Biosyst. Eng. 43 (7), 1279–1286. https://doi.org/10.1007/s00449-020-02324-6
Cao, L., Lu, W., Mata, A., Nishinari, K., Fang, Y., 2020. Egg-box model-based gelation of alginate and pectin: a review. Carbohydr. Polym. 242. https://doi.org/10.1016/j.carbpol.2020.116389
Carvalho, P.H., Kawaguti, H.Y., de Souza, W.F.C., Sato, H.H., 2021. Immobilization of Serratia plymuthica by ionic gelation and cross-linking with transglutaminase for the conversion of sucrose into isomaltulose. Bioprocess Biosyst. Eng. 0123456789. https://doi.org/10.1007/s00449-021-02513-x
Chiou, S.-H., Wu, W.-T., 2004. Immobilization of Candida rugosa lipase on chitosan with activation of the hydroxyl groups. Biomaterials 25 (2), 197–204. https://doi.org/10.1016/S0142-9612(03)00482-4
Collins, S.E., Lassalle, V., Ferreira, M.L., 2011. FTIR-ATR characterization of free Rhizomucor meihei lipase (RML), Lipozyme RM IM and chitosan-immobilized RML. J. Mol. Catal. B: Enzym. 72 (3–4), 220–228. https://doi.org/10.1016/j.molcatb.2011.06.009
Costa, H.P., de, S., da Silva, M.G.C., Vieira, M.G.A., 2021. Application of alginate extraction residue for Al(III) ions biosorption: a complete batch system evaluation. Environ. Sci. Pollut. Res. 28 (37), 51826–51840. https://doi.org/10.1007/s11356-021-14333-3
Costa, J.B., Lima, M.J., Sampaio, M.J., Neves, M.C., Faria, J.L., Morales-Torres, S., Tavares, A.P.M., Silva, C.G., 2019. Enhanced biocatalytic sustainability of laccase by immobilization on functionalized carbon nanotubes/polysulfone membranes. Chem. Eng. J. 355, 974–985. https://doi.org/10.1016/j.cej.2018.08.178
Daemi, H., Barikani, M., 2012. Synthesis and characterization of calcium alginate nanoparticles, sodium homopolymannuronate salt and its calcium nanoparticles. Sci. Iran. 19 (6), 2023–2028. https://doi.org/10.1016/j.scient.2012.10.005
Deze, E.G., Papageorgiou, S.K., Favvas, E.P., Katsaros, F.K., 2012. Porous alginate aerogel beads for effective and rapid heavy metal sorption from aqueous solutions: Effect of porosity in Cu2+ and Cd2+ ion sorption. Chem. Eng. J. 209, 537–546. https://doi.org/10.1016/j.cej.2012.07.133
Dumas, J.B.A., 1831. Procedes de l'analyse Organic. Ann. De. Chim. Et. Phys. 247, 198–213.
Facin, B.R., Valério, A., Bresolin, D., Centenaro, G., de Oliveira, D., Oliveira, J.V., 2018. Improving reuse cycles of Thermomyces lanuginosus lipase (NS-40116) by immobilization in flexible polyurethane. Biocatal. Biotransform. 36 (5), 372–380. https://doi.org/10.1080/10242422.2018.1458842
Facin, B.R., Melchiors, M.S., Valério, A., Oliveira, J.V., Oliveira, D. de, 2019. Driving immobilized lipases as biocatalysts: 10 years state of the art and future prospects. Ind. Eng. Chem. Res. 58 (14), 5358–5378. https://doi.org/10.1021/acs.iecr.9b00448
Fojan, P., 2000. What distinguishes an esterase from a lipase: a novel structural approach. Biochimie 82 (11), 1033–1041. https://doi.org/10.1016/S0300-9084(00)01188-3
Foresti, M.L., Valle, G., Bonetto, R., Ferreira, M.L., Briand, L.E., 2010. FTIR, SEM and fractal dimension characterization of lipase B from Candida antarctica immobilized onto titania at selected conditions. Appl. Surf. Sci. 256 (6), 1624–1635. https://doi.org/10.1016/j.apsusc.2009.09.083
Ghide, M.K., Li, K., Wang, J., Abdulmalek, S.A., Yan, Y., 2022. Immobilization of Rhizomucor miehei lipase on magnetic multiwalled carbon nanotubes towards the synthesis of structured lipids rich in sn-2 palmitic acid and sn-1,3 oleic acid (OPO) for infant formula use. Food Chem. 390, 133171. https://doi.org/10.1016/j.foodchem.2022.133171
Guisan, J.M., Fernandez-lorente, G., Rocha-martin, J., Moreno-gamero, D., 2022. ScienceDirect Enzyme immobilization strategies for the design of robust and efficient biocatalysts. Curr. Opin. Green. Sustain. Chem. 35, 100593. https://doi.org/10.1016/j.cogsc.2022.100593
Imam, H.T., Marr, P.C., Marr, A.C., 2021. Enzyme entrapment, biocatalyst immobilization without covalent attachment. Green. Chem. 23 (14), 4980–5005. https://doi.org/10.1039/D1GC01852C
Kabir, I.I., Sorrell, C.C., Mofarah, S.S., Yang, W., Yuen, A.C.Y., Nazir, M.T., Yeoh, G.H., 2020. Alginate/polymer-based materials for fire retardancy: synthesis, structure, properties, and applications. Polym. Rev. https://doi.org/10.1080/15583724.2020.1801726
Kazan, A., Heymuth, M., Karabulut, D., Akay, S., Yildiz-Ozturk, E., Onbas, R., Muderrisoglu, C., Sargin, S., Heils, R., Smirnova, I., Yesil-Celiktas, O., 2017. Formulation of organic and inorganic hydrogel matrices for immobilization of β-glucosidase in microfluidic platform. Eng. Life Sci. 17 (7), 714–722. https://doi.org/10.1002/elsc.201600218
Khoo, K.-M., Ting, Y.-P., 2001. Biosorption of gold by immobilized fungal biomass. Biochem. Eng. J. 8 (1), 51–59. https://doi.org/10.1016/S1369-703X(00)00134-0
Kumar, S., Haq, I., Prakash, J., Raj, A., 2017. Improved enzyme properties upon glutaraldehyde cross-linking of alginate entrapped xylanase from Bacillus licheniformis. Int. J. Biol. Macromol. 98, 24–33. https://doi.org/10.1016/j.ijbiomac.2017.01.104
Liu, S., 2020. Mass transfer effects: immobilized and heterogeneous reaction systems. Bioprocess Engineering. Elsevier, pp. 773–817. https://doi.org/10.1016/B978-0-12-821012-3.00017-8
Miranda, L.P., Guimarães, J.R., Giordano, R.C., Fernandez-Lafuente, R., Tardioli, P.W., 2020. Composites of crosslinked aggregates of eversa® transform and magnetic nanoparticles. Performance in the ethanolysis of soybean oil. Catalysts 10 (8), 817. https://doi.org/10.3390/catal10080817
de Moura, S.C.S.R., Berling, C.L., Germer, S.P.M., Alvim, I.D., Hubinger, M.D., 2018. Encapsulating anthocyanins from Hibiscus sabdariffa L. calyces by ionic gelation: pigment stability during storage of microparticles. Food Chem. 241, 317–327. https://doi.org/10.1016/j.foodchem.2017.08.095
Neves Petersen, M.T., Fojan, P., Petersen, S.B., 2001. How do lipases and esterases work: the electrostatic contribution. J. Biotechnol. 85 (2), 115–147. https://doi.org/10.1016/S0168-1656(00)00360-6
Nwagu, T.N., Okolo, B., Aoyagi, H., 2021. Immobilization of raw starch saccharifying amylase on glutaraldehyde activated chitin flakes increases the enzyme operation range. Bioresour. Technol. Rep. 13, 100645. https://doi.org/10.1016/j.biteb.2021.100645
Paulo, B.B., Ramos, F., de, M., Prata, A.S., 2017. An investigation of operational parameters of jet cutting method on the size of Ca-alginate beads. J. Food Process Eng. 40 (6), e12591. https://doi.org/10.1111/jfpe.12591

Pereira, da S., L. Fraga, A., M. Diniz, J., C. Fontes-Sant'Ana, G, M., Amaral, P, F.F., 2018. High catalytic activity of lipase from yarrowia lipolytica immobilized by microencapsulation. Int. J. Mol. Sci. 19 (11), 3393. https://doi.org/10.3390/ijms19113393

Prüße, U., Fox, B., Kirchhoff, M., Bruske, F., Breford, J., Vorlop, K.D., 1998a. New process (jet cutting method) for the production of spherical beads from highly viscous polymer solutions. Chem. Eng. Technol. 21 (1), 29–33. https://doi.org/10.1002/(SICI)1521-4125(199801)21:1<29::AID-CEAT29>3.0.CO;2-Y

Prüße, U., Fox, B., Kirchhoff, M., Bruske, F., Breford, J., Vorlop, K.D., 1998b. The jet cutting method as a new immobilization technique. Biotechnol. Tech. 12 (2), 105–108. https://doi.org/10.1023/A:1008828214839

Prüße, U., Jahnz, U., Wittlich, P., Breford, J., and Vorlop, K. (2002). Aus dem Institut für Technologie und Biosystemtechnik Ulf Prüße Peter Wittlich Klaus-Dieter Vorlop Ulrich Jahnz Jürgen Breford Bead production with JetCutting and rotating disk / nozzle technologies Manuskript, zu finden in www.fal.de Braunschweig Bundes. 1–10.

Rafiee, F., Rezaee, M., 2021. Different strategies for the lipase immobilization on the chitosan based supports and their applications. Int. J. Biol. Macromol. 179, 170–195. https://doi.org/10.1016/j.ijbiomac.2021.02.198

Remonatto, D., Miotti Jr., R.H., Monti, R., Bassan, J.C., de Paula, A.V., 2022. Applications of immobilized lipases in enzymatic reactors: a review. Process Biochem. 114, 1–20. https://doi.org/10.1016/j.procbio.2022.01.004

Riley, M.R., Muzzio, F.J., Reyes, S.C., 1997. Effect of oxygen limitations on monoclonal antibody production by immobilized hybridoma cells. Biotechnol. Prog. 13 (3), 301–310. https://doi.org/10.1021/bp970028n

Rodrigues, M.I., Iemma, A.F., 2014. Experimental Design and Process Optimization, first ed. CRC Press.

Sheldon, R.A., van Pelt, S., 2013. Enzyme immobilisation in biocatalysis: why, what and how. Chem. Soc. Rev. 42 (15), 6223–6235. https://doi.org/10.1039/c3cs60075k

Silva, T.L., da, Silva, M.G.C. da, Vieira, M.G.A., 2021. Palladium adsorption on natural polymeric sericin-alginate particles crosslinked by polyethylene glycol diglycidyl ether. J. Environ. Chem. Eng. 9 (4), 105617. https://doi.org/10.1016/j.jece.2021.105617

Silverio, G.B., Sakanaka, L.S., Alvim, I.D., Shirai, M.A., Grosso, C.R.F., 2018. Production and characterization of alginate microparticles obtained by ionic gelation and electrostatic adsorption of concentrated soy protein. Ciência Rural 48 (12). https://doi.org/10.1590/0103-8478cr20180637

Simón-Herrero, C., Naghdi, M., Taheran, M., Kaur Brar, S., Romero, A., Valverde, J.L., Avalos Ramirez, A., Sánchez-Silva, L., 2019. Immobilized laccase on polyimide aerogels for removal of carbamazepine. J. Hazard. Mater. 376, 83–90. https://doi.org/10.1016/j.jhazmat.2019.05.032

de Souza, W.F.C., de Castro, R.J.S., Sato, H.H., 2022. Sequential optimization strategy for the immobilization of Erwinia sp. D12 cells and the production of isomaltulose with high stability and prebiotic potential. Bioprocess Biosyst. Eng. 45 (6), 999–1009. https://doi.org/10.1007/s00449-022-02719-7

Wu, W.D., Patel, K.C., Rogers, S., Chen, X.D., 2007. Monodisperse droplet generators as potential atomizers for spray drying technology. Dry. Technol. 25 (12), 1907–1916. https://doi.org/10.1080/07373930701727176

Yagar, H., Balkan, U., 2017. Entrapment of laurel lipase in chitosan hydrogel beads. Artif. Cells, Nanomed., Biotechnol. 45 (5), 864–870. https://doi.org/10.1080/21691401.2016.1182920

Zhang, Z., Zhang, R., Zou, L., McClements, D.J., 2016. Protein encapsulation in alginate hydrogel beads: effect of pH on microgel stability, protein retention and protein release. Food Hydrocoll. 58, 308–315. https://doi.org/10.1016/j.foodhyd.2016.03.015